Accepted Manuscript

Structure and microwave dielectric properties of glass free low temperature Co-firable $SrMV_2O_7$ (M=Mg, Zn) ceramics

E.K. Suresh, R. Ratheesh

PII: S0925-8388(19)32868-3

DOI: https://doi.org/10.1016/j.jallcom.2019.07.353

Reference: JALCOM 51641

To appear in: *Journal of Alloys and Compounds*

Received Date: 16 April 2019

Revised Date: 27 July 2019

Accepted Date: 29 July 2019

Please cite this article as: E.K. Suresh, R. Ratheesh, Structure and microwave dielectric properties of glass free low temperature Co-firable $SrMV_2O_7$ (M=Mg, Zn) ceramics, *Journal of Alloys and Compounds* (2019), doi: https://doi.org/10.1016/j.jallcom.2019.07.353.

Structure and Microwave Dielectric Properties of Glass Free Low Temperature Co-firable $SrMV_2O_7$ (M=Mg, Zn) Ceramics

E.K. Suresh[a], R. Ratheesh[b*]

[a]Microwave Materials Group, Centre for Materials for Electronics Technology (C-MET), Ministry of Electronics and Information Technology, Government of India, Thrissur, Kerala, India-680581,

[b]Centre for Materials for Electronics Technology (C-MET), Ministry of Electronics and Information Technology, Government of India, Hyderabad, Telangana, India- 500051

*Corresponding author

Tel.: +91-040-27265673; fax: +91-040-27261658

*E-mail address:*ratheesh@cmet.gov.in.

Abstract

$SrZnV_2O_7$ (SZV) and $SrMgV_2O_7$ (SMV) ceramics have been prepared through solid state ceramics route. The crystal structure of the ceramics was studied in detail using X-ray diffraction and Raman spectroscopic techniques. Both the ceramics show good microstructure and microwave dielectric properties. Among the samples studied, $SrZnV_2O_7$ ceramic sintered in the ultra low temperature of 660°C for 1h and it shows ε_r=10.2, Q×f=31900GHz, τ_f= -76ppm/°C together with excellent chemical compatibility with Aluminium and Silver metal electrodes. $SrMgV_2O_7$ ceramic sintered at an optimum temperature of 780°C for 1h exhibits ε_r=16, Q×f=21300GHz, τ_f= -70ppm/°C and shows chemical reactivity with silver metal electrode.

Keywords: Ceramics; Crystal structure; Dielectric response; Scanning electron microscopy, SEM; X-ray diffraction

1. Introduction

Modern electronic circuit fabrication industry witnessed revolutionary changes for the past few decades. Smaller, lighter and high operating frequency circuits are required for the fabrication of small size and more functional electronic devices. Multilayer circuit fabrication technique is used to meet these requirements. Low temperature co-fired ceramic (LTCC) technology has been widely used in multilayer circuit manufacturing because of its stable physical and electronic properties, ease of fabrication and high density circuit packaging. LTCC devices have also been used in military and radar applications because of its design flexibility and high reliability. LTCC technology is more preferred in high frequency applications since the traditional PCB technology suffer from higher dielectric loss as frequency increases. Therefore the development of low loss and low temperature co-firable ceramic material systems is of high demand to cater to this requirement.

For the past decade, large number of V_2O_5[1-5] and MoO_3 [6-8] based low loss ceramic materials were reported in literature for LTCC applications. Recently Ultra low temperature co-fired ceramics (ULTCC) were also got much attention so as to use Aluminium (Al) as the conducting electrodes [9-13]. Among the available reports, V_2O_5 based ceramic materials were found promising candidates for LTCC and ULTCC applications owing to their high quality factor, better chemical stability and superior chemical compatibility with metal electrodes. The BaO-V_2O_5 is one of the very well studied binary phase diagrams. BaV_2O_6, $Ba_2V_2O_7$, $Ba_3V_2O_8$ and $Ba_3V_4O_{13}$ were reported as stable single phase compositions in this phase diagram [14]. Our group reported the microwave dielectric properties of BaV_2O_6 and $Ba_3V_4O_{13}$ ceramics for ULTCC applications [15,16]. Umemura et.al reported that $Ba_3V_2O_8$ ceramic sintered at 1600°C for 5h shows excellent microwave dielectric properties. The authors also reported that B_2O_3

addition significantly reduces the sintering temperature of $Ba_3V_2O_8$ ceramic and it can be used as an appropriate material for LTCC applications [17]. Joung et.al reported the formation process and microwave dielectric properties of $R_2V_2O_7$ (R= Ba, Sr and Ca) ceramics [18]. Recently Fang et.al reported the microwave dielectric properties of low firing double pyrovanadates in the BaO-MO- V_2O_5 (M=Mg,Zn) system. $BaMgV_2O_7$ and $BaZnV_2O_7$ ceramics sintered at optimum temperatures possess microwave dielectric properties of ε_r = 8.2 and 10.7, Q×f = 37600 and 31000GHz and τ_f= -35.2 and -64.4 ppm/°C respectively [19].

The crystal structure of other alkaline earth double pyrovanadates such as $SrZnV_2O_7$, $SrMgV_2O_7$, $CaMgV_2O_7$, $CaZnV_2O_7$ etc. were also reported in literature [20-23]. The photoluminescence characteristics of Eu^{3+} and Sm^{3+} doped $SrZnV_2O_7$ nanocrystals were well studied by Dalal et.al.[24,25]. Photocatalytic activities of pure and Ni^{2+} doped $CaZnV_2O_7$ were studied by Wang et.al [26]. The microwave dielectric properties of these double pyrovanadates are not studied in detail. In the present work, we investigate the structure and microwave dielectric properties $SrMV_2O_7$ (M=Mg, Zn) double pyrovanadates. A detailed study on the chemical compatibility of these ceramics with metal electrodes was also carried out to ascertain the suitability of these materials for LTCC and ULTCC applications.

2. Experimental procedure

The $SrMV_2O_7$ (M=Mg, Zn) ceramics were prepared through solid state ceramic route. High purity $SrCO_3$ (99%, Himedia), MgO (99%, Sigma Aldrich), ZnO (99.9%, Sigma Aldrich) and V_2O_5 (99.6%, Sigma Aldrich) were used as the starting materials. The stoichiometric amounts of oxides and carbonates were weighed and wet mixed in distilled water for about an hour and then dried in a hot air oven at 80°C. The $SrMV_2O_7$ (M=Mg, Zn) ceramics were calcined at 650 and 600°C for 4 h respectively in a programmable SiC furnace. The calcined compositions

were ground in to fine powders and 5 wt% polyvinyl alcohol (PVA) solution was added to these powders and then dried. The powders were again ground well and pressed uniaxially in a tungsten carbide die of 11 mm diameter by applying a pressure of 250 MPa. The cylindrical compacts of $SrMV_2O_7$ (M=Mg, Zn) samples were sintered at 780 and 660°C for 1 h respectively. The density of the sintered pellets was determined using dimensional method. The kinetics of phase formation of the ceramics was studied using TGA/DSC analyses (TGA-DSC, SDT, Q600 TA Instrument) with a heating rate of 5°/min in a nitrogen atmosphere. The phase purity of the specimens was analyzed using X-ray diffraction technique (M/s Rigaku, Ultima,). Rietveld refinement was performed using GSAS suite with EXPGUI [27,28]. Raman spectra of $SrMV_2O_7$ (M=Mg, Zn) ceramics were recorded using a WITech Alpha 300RA confocal Raman microscope with DPSS laser of 532 nm. The sintered ceramic compacts were thermally etched at a temperature 100°C less than that of the sintering temperature for SEM characterization. The back scattered electron images and EDS analysis of the samples were studied using scanning electron microscope interfaced with EDS system (Carl Zeiss, Model No: EVO18 Research, Germany). The linear thermal expansion coefficient of the ceramics were studied in the temperature range 30-300 $^{\circ}$C using a EXSTAR 6000 model thermo mechanical analyzer (SII Nano technology INC., Japan).The dielectric constant and the unloaded quality factor of the sintered samples were studied by Hakki and Coleman [29] post resonator technique and resonant cavity method [30] respectively, using a Vector Network Analyzer (Agilent, E8362b, USA). The temperature coefficient of resonant frequency (τ_f) was measured in the temperature range 30-100 $^{\circ}$C.

3. Results and discussion

The phase formation process of $SrZnV_2O_7$ (SZV) and $SrMgV_2O_7$ (SMV) ceramics are studied using thermo gravimetric (TG) and differential scanning calorimetric (DSC) analyses at nitrogen atmosphere with a heating rate of 5° per minute and the results are shown in fig 1(a-b). The endotherms and associated weight loss observed below 200°C is due to the evaporation of water molecules. The sharp endotherm below 200°C and associated weight loss in TGA for SMV, as compared to SZV, due to more amount of adsorbed water molecules in the former. The exotherms observed in the temperature range 300-450°C without weight loss for both the compositions indicate the chemical reactions taken place during the formation of the respective compositions. The endotherms and associated weight loss in the temperature range 450 to 650°C in SZV ceramic depicts the evaporation of volatile impurities and formation of the final composition. Whereas, in SMV the formation of the final composition is observed at slightly higher temperature range.

The powder X-ray diffraction patterns of $SrZnV_2O_7$ (SZV) and $SrMgV_2O_7$ (SMV) ceramics are given in fig 2 and 3 respectively. In order to confirm the phase formation Rietveld refinement was carried out on both the XRD patterns using GSAS suite with EXPGUI. The Rietveld refinement parameters R_{wp}, R_p and χ^2 obtained for SZV and SMV ceramics are 7.6%, 4.25%, 1.15 and 10.6%, 8%, 1.63 respectively. The inset of fig 2 and 3 shows the unit cell representation of SZV and SMV ceramics. SZV having monoclinic crystal structure with space group $P2_1/n$ (14). The refined lattice parameters for SZV ceramics are a=7.419Å, b=6.699Å, c=11.971Å and β=95.99° respectively. The Zn atoms are coordinated with five oxygen atoms to form ZnO_5 trigonal bipyramids. V(1) and V(2) atoms are tetrahedrally coordinated with four

oxygen atoms to form VO_4 groups. The $V(1)O_4$ and $V(2)O_4$ tetrahedral units are connected with corner sharing oxygen atoms to form V_2O_7 pyrogroups [20,31].

SMV also crystallizes in the monoclinic structure with $P2_1/c$ (14) space group. The refined lattice parameters for SMV ceramic are a=6.741Å, b=14.661Å, c=11.159Å and β=98.94°. The magnesium atoms are octahedrally coordinated with oxygen atoms, which is edge sharing with one another to form Mg_2O_{10} dimers. V(1) and V(2) atoms are coordinated with five oxygen atoms, which are connected together by edge sharing O1 and O5 atoms. These vanadium-oxygen polyhedra is connected with $V(3)O_4$ and $V(4)O_4$ tetrahedral units by corner sharing O3 and O7 atoms to form V_4O_{14} chains [21,23,32,33].

Raman spectroscopy is an effective tool to analyze the vibrational characteristics of molecules. The Raman spectra of SZV and SMV ceramics are given in fig.4. SZV ceramic crystallizes in the monoclinic structure, $P2_1/n$ space group with four formula units in the crystallographic unit cell which corresponds to C_{2h} point group. In SZV ceramic all the atoms are in 4e Wyckoff's position and occupy in the C_1 site symmetry. The total number of vibrations at the Brillouin zone center after eliminating the acoustic modes is given as

$$\Gamma = 33A_g+33B_g+32A_u+31B_u$$

Where A_g and B_g modes are Raman active. Even though 66 Raman active modes are obtained theoretically, lesser number of modes is observed in the Raman spectrum. Similar observation was also reported by Rakhi et.al [34]. The authors reported that the reduced number of peaks may be due to the poly crystalline nature of sample, overlapping of bands etc.. The crystal structure of SZV consists of V_2O_7 pyrogroups formed by corner sharing oxygen atoms of VO_4 tetrahedral units. Hence the internal vibrations of VO_3 end group and V-O-V bridge vibrations

are expected in the Raman spectra of SZV ceramics. The strong peaks observed at 896 and 935 cm^{-1} are due to the symmetric stretching vibrations of VO_3 groups. The Raman bands in the region 785 to 862 cm^{-1} are due to the asymmetric stretching vibrations of VO_3 groups. The symmetric stretching and asymmetric stretching vibrations of V-O-V bridges are observed in the region 571 to 715 cm^{-1}. The bands observed in the range 304 to 398 cm^{-1} are due to the symmetric and asymmetric bending vibrations of VO_3 groups**.** The Raman peaks observed at 223 and 263 cm^{-1} may be due to the bending vibrations of V-O-V bridges and O-VO_3 groups respectively. The Raman bands obtained below 190 cm^{-1} is due to the lattice mode vibrations [35-41].

SMV ceramics also crystallizes in the monoclinic structure with $P2_1/C$ (14) space group having 8 molecules in the crystallographic unit cell. All the atoms occupy in the 4e Wyckoff's position and the possible site symmetry is C_1. According to Factor group analysis, the total number of vibrations in the Brillouin zone center after eliminating the acoustic modes is given as

$$\Gamma = 66A_g+66B_g+65A_u+64B_u$$

Where Ag and Bg modes are Raman active. The crystal structure of SMV composed of V_4O_{14} groups consists of two edge shared VO_5 bipyramid which are corner connected with two VO_4 tetrahedra. Hence the internal vibrations of VO_5 and VO_3 groups are expected in SMV ceramics. According to factor group analysis more number of peaks expected in the Raman spectrum of SMV compared to SZV ceramics. In order to determine the number of stretching modes, the Raman spectra of SZV and SMV ceramics are deconvoluted in the 700 to 1100 cm^{-1} and results are given in fig 5. As expected, more number of stretching modes observed in SMV ceramics indicates the different vanadium oxygen linkages. Eight vibrational modes are observed in the

700 to 1100 cm^{-1} against six in the case of SZV ceramic. The more number of internal modes observed in the SMV ceramic is due to different V-O bond lengths exist as a result of VO_5 bipyramids and corner connected VO_4 tetrahedra in the V_4O_{14} groups. Unlike SZV, the Raman mode observed in the 1004 cm^{-1} in SMV ceramics may be due to the stretching vibration of V-O bond in the VO_5 bipyramid. The result agrees with the earlier reports [42-48]. The Raman peaks obtained in the higher wave number region of 794 to 913 cm^{-1} is due to the stretching vibrations of V-O bonds. Unlike V-O stretching vibrations, V-O-V bridging vibrations gave rise to less number of modes in SMV ceramic, which could be due to restricted V-O-V bridging vibration as a result of edge shared VO_5 groups. The Raman modes observed in the region of 298 to 421 cm^{-1} may be due to the terminal bending vibration of VO_3 groups. The Raman bands observed in the range 190 to 242 cm^{-1} can be attributed to the bending vibrations of V-O-V bridges and O-VO_3 groups. The modes observed below 190 cm^{-1} is due to the external modes [35-41]. Since the SMV ceramic consists of complex V_4O_{14} chains an unambiguous Raman band assignments in the external mode region is not possible.

Fig 6 shows the backscattered SEM images of SZV and SMV ceramics sintered at 660 and 780°C respectively. Well sintered polygonal grains with less amount of porosity are noticed for both the ceramics. SZV ceramic shows larger grain size as compared to SMV ceramic. No secondary phases are observed in the back scattered SEM images. The typical shrinkage behavior for SZV ceramic is given in fig 7. The shrinkage behavior is studied in the temperature range 30-600°C. The ceramic shows very good shrinkage in the temperature range of 500-600°C and among the samples studied SZV ceramic shows ultra low sinterability.

Coefficient of thermal expansion of LTCC ceramic plays an important role in circuit fabrication. In the present study, the coefficient of thermal expansion of SZV and SMV ceramics

are measured in the temperature range of 30-300°C and the results are given in fig8. The thermal expansion curves show linear variation with temperature and CTE values of 10.7 and 9.2 ppm/°C respectively are exhibited by SZV and SMV ceramics.

The optimum sintering temperature, density and microwave dielectric properties of SZV and SMV ceramics are given in table 1. The optimum sintering temperature obtained for SZV ceramic is 660°C for 1h. The sample sintered at this temperature exhibits a density value of 3.8 g/cm^3 together with ε_r=10.2 (f=9.351708(GHz), Q×f=31900GHz (f=7.965234GHz) and τ_f= -76 ppm/°C. The SMV ceramic sintered at an optimum sintering temperature of 780°C for 1h exhibits maximum density value of 3.48 g/cm^3 together with ε_r=16 (f=8.006500GHz), Q×f=21300GHz (f=7.101600GHz) and τ_f= -70 ppm/°C. SMV ceramic exhibits low quality factor as compared to SZV. This can be correlated with the intensity of Raman bands. SZV ceramic shows sharp stretching phonon mode as compared to SMV ceramic. Several authors reported the inverse relation between the width of Raman modes and Q×f values [49,50]. The FWHM values for maximum intense V-O stretching mode for SZV and SMV ceramics are 17 and 21 cm^{-1} respectively. In the present study ceramic with lowest FWHM shows highest quality factor, which agrees with the previous reports. Chen et al. reported that Raman peak width is correlated with the decay of microwave energy propagation. The sharp stretching mode indicates highly ordered and rigid oxygen cage structure. This increase the microwave energy propagation decay time and thereby the material possesses higher Q×f values [50].

Table 1 Sintering temperature, density and microwave dielectric properties of SZV and SMV ceramics

Composition	Sint. Temp	Density(g/cm^3)	ε_r	Q×f (GHz)	τ_f (ppm/°C)
SZV	660°C/1h	3.8	10.2	31900	-76
SMV	780°C/1h	3.48	16	21300	-70

Present study shows that SZV ceramic can be very well sintered in the ultra low temperature range. Since the sintering temperature of SZV ceramic is 660°C, both silver and aluminium compatibility studies have been carried out. In order study the chemical compatibility with silver and aluminium electrodes, 20 wt% of these metal powders were mixed with SZV ceramic and co-fired at 650°Cfor 1h. The XRD patterns of the co-fired samples are given in fig 9. In addition to the ceramic phase, the silver and aluminium peaks are separately observed in the XRD patterns indicating the chemical compatibility of these ceramics with metal electrodes.

In order to further affirm these results, EDS analyses have been carried out on the co-fired samples. Fig 10(a-e) shows the EDS spot, line scan and X-ray dot mapping results of SZV ceramic co-fired with aluminium electrodes. In spot1, the presence of metal electrode only is detected whereas ceramic phase without aluminium are observed in spot2 (fig 10a-c). EDS line scan results also show that there is no inter diffusion of aluminium metal in the ceramic phase (fig 10d). X-ray dot mapping image confirms the segregation of aluminium particles from ceramics (fig 10e). Similar results also observed for SZV ceramic co-fired with silver (fig 11a-e). These results further confirm the excellent chemical compatibility of SZV ceramic with aluminium and silver electrodes.

In order to study the suitability of SMV ceramic for LTCC applications, 20wt% Ag powder was added to the SMV ceramic and co-fired at 760°C for 1h. Fig 12 shows the XRD patterns of phase pure SMV ceramic and the Ag co-fired sample. In addition to some additional

peaks, intensity changes are also noticed in the co-fired XRD pattern. The silver peaks are not separately observed in the XRD pattern indicating the chemical reactivity between Ag metal and SMV ceramic. These results are further evaluated through EDS analysis. Fig 13(a-e) shows the EDS analysis results of SMV ceramic co-fired with Ag powder. EDS spectrum of spot1 consists of both Ag and ceramic phases, whereas only the presence of ceramic phase is noticed in spot 2 (fig 13a-c). EDS line scan results also show the reactivity between Ag and SMV ceramic (fig 13d). X-ray dot mapping image indicates that the silver is floated over the ceramic (fig 13e). Hence, it can be inferred from both XRD and EDS studies that SMV ceramic doesn't have chemical compatibility with Ag electrode during co-firing.

4. Conclusions

Phase pure SZV and SMV ceramics have been prepared through solid state ceramic route. The phase formation of the ceramics has been confirmed through TGA/DSC analysis. Rietveld refinement and Raman spectroscopic studies reveal that SZV ceramic consists of V_2O_7 pyrogroups formed from corner sharing VO_4 tetrahedra whereas SMV ceramic consists of V_4O_{14} chains. Both the ceramics show closely packed microstructure. SZV and SMV ceramics exhibit an average linear expansion coefficient of 10.7 and 9.2ppm/°C respectively in the temperature range 30-300°C. SZV ceramics can be well sintered in the ultra low temperature. SZV ceramic shows ε_r=10.2, Q×f=31900GHz, τ_f= -76ppm/°C at an optimum sintering temperature of 660°C for 1h. SMV ceramic exhibits ε_r=16, Q×f=21300GHz, τ_f= -70ppm/°C at an optimum sintering temperature of 780°C for 1h. The quality factor of SZV and SMV ceramics show an inverse relation with the FWHM of symmetric stretching modes. The sharp peaks of Raman bands for SZV ceramic compared to SMV indicates more rigid vanadium oxygen linkage in SZV ceramics. XRD and EDS analyses reveal that SZV ceramic has excellent chemical compatibility with Al

and Ag electrodes whereas SMV ceramic reacts with Ag electrodes. It is clearly evident from the present study that SZV ceramic can be used as a good candidate material for ULTCC applications.

Acknowledgements

The authors are thankful to Dr. N. Raghu, Director, C-MET, Thrissur for extending the facilities to carry out the work. The authors are also thankful to the Board of Research in Nuclear Sciences, Mumbai for financial support under grant number 34/15/01/2014-BRNS/0906. The authors are thankful to DST SAIF, M. G. University, Kottayam for Raman analyses. One of the authors, E.K.Suresh is grateful to the Council of Scientific and Industrial Research (CSIR), India for the award of Senior Research Fellowship.

References

[1] Umemura, R.; Ogawa, H.; Ohsato, H.; Kan, A.; Yokoi, A. Microwave Dielectric properties of Low-Temperature Sintered $Mg_3(VO_4)_2$ Ceramic, *J. Eur. Ceram. Soc.* **2005,** 25, 2865-2870.

[2] Suresh, E. K.; Unnimaya, A. N.; Surjith, A.; Ratheesh, R. New Vanadium Based $Ba_3MV_4O_{15}$ (M=Ti and Zr) high Q ceramics for LTCC applications, *Ceram. Int.* **2013,** 39, 3635-3639.

[3] Fang, L.; Xiang, F.; Su, C.; Zhang, H. A Novel Low Firing Microwave Dielectric Ceramic $NaCa_2Mg_2V_3O_{12}$, *Ceram. Int.* **2013,** 39, 9779-9783.

[4] Suresh, E. K.; Prasad, K.; Arun, N. S.; Ratheesh, R. J. Synthesis and Microwave Dielectric Properties of $A_{16}V_{18}O_{61}$ (A= Ba, Sr and Ca) Ceramics for LTCC Applications, *Electron. Mater.* **2016,** 45, 2996-3002.

[5] Unnimaya, A. N.; Suresh, E. K.; Ratheesh, R. Crystal Structure and Microwave Dielectric Properties of New Alkaline Earth Vanadate $A_4V_2O_9$ (A = Ba, Sr, Ca, Mg and Zn) Ceramics for LTCC Applications, *Mater .Res. Bull.* **2017,** 88, 174-181.

[6] Surjith, A.; Suresh, E. K.; Freddy, S.; Ratheesh, R. Microwave Dielectric Properties of Low Temperature Sinterable $RE_2Mo_4O_{15}$ (RE 5 Nd, Sm) Ceramics for LTCC Applications, *J. Mater. Sci. Mater. Electron.* **2013,** 24, 1818-1822.

[7] Surjith, A.; Ratheesh, R. High Q Ceramics in the $ACe_2(MoO_4)_4$ (A = Ba, Sr and Ca) System for LTCC Applications, *J. Alloy. Compd.* **2013,** 550, 169-172.

[8] Xi, H.; Zhou, D.; Xie, H.; W. Li. Microwave Dielectric Properties of Low Firing Scheelite-Related $(Na_{0.5}La_{0.5})MoO_4$ Ceramic, *Mater. Lett.* **2015,** 142, 221-224.

[9] Xiang, H.; Tang, Y.; Fang, L.; Porwal, H.; Li, C. J. A Novel Ultra-Low Temperature Co-fired $Na_2BiZn_2V_3O_{12}$ Ceramic and its Chemical Compatibility with Metal Electrodes, *Mater. Sci. Mater. Electron.* **2016,** 28, 1508-1513.

[10] Chen, J.; Li, C.; Xiang, H.; Tang, Y.; Fang, L. SrV_2O_6: An Ultra low-Firing Microwave Dielectric Ceramic for LTCC Applications, *Mater .Res. Bull.* **2018,** 100, 377-381.

[11] Dhanya, J.; Basiluddeen, A. V.; Ratheesh, R. Synthesis of Ultra Low Temperature Sinterable $Na_2Zn_5(MoO_4)_6$ Ceramics and the Effect of Microstructure on Microwave Dielectric Properties, *Scrip. Mater.* **2017,** 132, 1-4.

[12] Pang, L. X.; Zhou, D.; Guo, J.; Yue, Z. X.; Yao, X. Microwave Dielectric Properties of $(Li_{0.5}Ln_{0.5})MoO_4$ (Ln = Nd, Er, Gd, Y, Yb, Sm, and Ce) Ceramics, *J. Am. Ceram. Soc.* **2015,** 98, 130-135.

[13] Dhanya, J.; Suresh, E. K.; R. Naveenraj, R.; Ratheesh, R. Synthesis and Characterization of $Na_5M(MoO_4)_4$ (M = Y,Yb) Microwave Ceramics for ULTCC Applications, *Ceram. Int.* **2018,** 44, 6699-6704.

[14] Fotieve, A. A.; Makarov, V. V.; Volkov, V. L.; Surat, L. L. The $BaO-V_2O_5$ System, *Russ. J. Inorg. Chem.* **1969,** 14, 144-146.

[15] Unnimaya, A. N.; Suresh, E. K.; Ratheesh, R. Structure and Microwave Dielectric Properties of Ultralow-Temperature Cofirable BaV_2O_6 Ceramics, *Eur. J. Inorg. Chem.* **2015,** 2015, 305-310.

[16] Suresh, E. K.; Unnimaya, A. N.; Ratheesh, R. Microwave Dielectric Properties of Ultralow-Temperature Cofirable $Ba_3V_4O_{13}$ Ceramics, *J. Am. Ceram. Soc.* **2014,** 97, 1530-1533.

[17] Umemura, R.; Ogawa, H.; Yokoi, A.; Ohsato, H.; Kan, A. Low-Temperature Sintering-Microwave Dielectric Property Relations in $Ba_3(VO_4)_2$ Ceramic, *J. Alloy. Compd.* **2006,** 424, 388-393.

[18] Joung, M. R.; Kim, J. S.; Song, M. E.; Nahm, S. Formation Process and Microwave Dielectric Properties of the $R_2V_2O_7$ (R=Ba, Sr, and Ca) Ceramics, *J. Am. Ceram. Soc.* **2009,** 92, 3092-3094.

[19] Fang, L.; Wei, Z.; Su, C.; Xiang, F.; Zhang, H. Novel Low-Firing Microwave Dielectric Ceramics: $BaMV_2O_7$ (M=Mg, Zn), *Ceram. Int.* **2014,** 40, 16835-16839.

[20] Velikodnyj, Y. A.; Murashova, E. V.; Trunov, V. K.; Crystal Structure of Double Pyrovanadate $SrZnV_2O_7$, *Kristallografiya.* **1989,** 34, 607-610.

[21] Velikodnyj, Y. A.; Trunov, V. K.; Kudin, O. V.; Zhuravlev, V. D.; Crystal Structure of Double Pyrovanadate of Strontium and Magnesium $SrMgV_2O_7$, *Kristallografiya.* **1985,** 30, 663-667.

[22] Murashova, E. V.; Velikodnyj, Y. A.; Zhuravlev, V. D.; Crystal Structures of Double Pyrovanadates $CaMgV_2O_7$ and $CaCoV_2O_7$, *Zh. Neorg. Khim.* **1993,** 38, 1453-1454.

[23] Babaryk, A. A.; Odynets, I. V.; Khainakov, S.; Granda, S. G.; Slobodyanik, N. S. Polyanionic Identity Of $Ca_2Zn_2(V_3O_{10})(VO_4)$ Photocatalyst Manifested by X-ray Powder Diffraction and Periodic Boundary Density Functional Theory Calculations, *Cryst. Eng. Comm.* **2015,** 17, 7772-7777.

[24] Dalal, M.; Taxak, V. B.; Lohra, S.; Sangwan, D.; Khatkar, S. P. Photoluminescence and Structural Properties of Eu^{3+} Doped $SrZnV_2O_7$ Nanocrystals, *J. Lumin.* **2015,** 161, 63-70.

[25] Dalal, M.; Taxak, V. B.; Chahar, S.; Khatkar, A.; Khatkar, S. P.; A Promising Novel Orange–Red Emitting $SrZnV_2O_7:Sm^{3+}$ Nanophosphor for Phosphor-Converted White LEDs with Near-Ultraviolet Excitation, *J. Phys. Chem. Solids.* **2016,** 89, 45-52.

[26] Wang, J.; Qin, L.; Huang, Y.; Cai, P.; Seo, H. J. Preparation and Photocatalytic Activities of Pyrovanadate $CaZnV_2O_7$ Under Visible Light Irradiation, *Matter. Lett.* **2014,** 125, 89-91.

[27] Larson A. C.; Von Dreele, R. B. GSAS General Structure Analysis System, Los Alamos National Laboratory Report, *LAUR.* **1994,** 86-748.

[28] Toby, B. H. J. EXPGUI, A Graphical User Interface for GSAS, *Appl. Cryst.* **2001,** 34, 210-213.

[29] Hakki, B. W.; Coleman. P. D. A Dielectric Resonator Method of Measuring Inductive Capacities in the Millimeter Range, *IRE. Trans. Microwave. Theory. Techn.* **1960,** 8, 402-410.

[30] Krupka, J.; Derzakowski, K.; Riddle, B.; Jarvis. J. B. A Dielectric Resonator for Measurements of Complex Permittivity of Low Loss Dielectric Materials as a Function of Temperature, *J. Meas. Sci. Technol.* **1998,** 9, 1751-1756.

[31] Guan, Y.; Huang, Y.; Tsuboi, T.; Huang, W.; Chen, C.; Cai, P.; Seo, H. J. Conversion and Quantum Efficiency from Ultraviolet Light to Near Infrared Emission in Yb^{3+} Doped Pyrovanadates $MZnV_2O_7$(M = Ca, Sr, Ba), *Mater. Sci. Eng.B.* **2014,** 190, 26-32.

[32] Zhuravlev, V. D.; Tyutyunnik, A. P.; Chufarov, A. Y.; lobachevskaya, N. I.; Velikodnyi, A. A. Crystal Structure of $Ca_2Zn_2(V_4O_{14})$ and $Pb_2Cd_2(V_3O_{10})(VO_4)$ Double Vanadates, *Powder diffraction.* **2018,** 33, 216-224.

[33] Smith Pellizzeri, T. M.; McMillen, C. D.; Pellizzeri, S.; Wen, Y.; Getman, R. B; Chumanov, G.; Kollis, J. W. Strontium Manganese Vanadates from Hydrothermal Brines: Synthesis and Structure of $Sr_2Mn_2(V_3O_{10})(VO_4)$, $Sr_3Mn(V_2O_7)_2$, and $Sr_2Mn(VO_4)_2(OH)$, *J. Solid. State. Chem.* **2017,** 255, 225-233.

[34] Rakhi, M.; Subodh, G. Crystal Structure and Microwave Dielectric Properties of $NaPb_2B_2V_3O_{12}$ (B=Mg, Zn) Ceramics, *J. Eur. Ceram. Soc.* **2018,** 38, 4962-4966.

[35] Baran, E. J.; Botto, I. L.; Pedregosa, J. C.; Aymonino, P. J. The Vibrational Spectrum of $Sr_2V_2O_7$ and the Vibrational Properties of the Divanadate Ion, *J. Monat. Fur. Chem.* **1978,** 109, 41-51.

[36] Unnimaya, A. N.; Suresh, E. K.; Dhanya, J.; Ratheesh, R. Structure and Microwave Dielectric Properties of $5BaO–2V_2O_5$ Binary Ceramic System, *J. Mater. Sci: Mater. Electron.* **2014,** 25, 1127-1131.

[37] Sallemi, F.; Megdiche, M.; Louati, B.; Guidara, K. Electrical Properties and Complex Impedance Analysis of $K_2ZnV_2O_7$, *Ind. J. Phy.* **2014,** 88, 1251-1256

[38] Naveenraj, R.; Suresh, E. K.; Dhanya, J.; Ratheesh, R. Preparation and Microwave Dielectric Properties of $Ba_3A(V_2O_7)_2$ (A = Mg, Zn) Ceramics for ULTCC Applications, *Eur. J. Inorg. Chem.* **2019,** 2019, 949-955.

[39] Busca, G.; Ricchiardi, G.; Hew Sam, D. S.; Volta, J. C. Spectroscopic Characterization of Magnesium Vanadate Catalysts Part 1 .-Vibrational Characterization of $Mg_3(VO_4)_2$ $Mg_2V_2O_7$, and MgV_2O_6, Powders, *J. Chem. Soc. Faraday. Trans.* **1994,** 90, 1161-1170.

[40] Schwendt, P.; Joniakova, D. Vibrational Spectra of Vanadium (V) Compounds. II. Vibrational Spectra of Divanadates with Nonlinear Bridge VOV, *Chem. Zvesti.* **1975,** 29, 381-386.

[41] Botto, I.L.; Baran, E. J.; Pedregosa, J. C.; Aymonino, P. J. The Vibrational Spectrum of Barium Divanadate, *Monatshefte. Fur. Chemie.* **1979,** 110, 895-898.

[42] Attos, O.; Massot, M.; Balkaski, M.; Poniatowski, E. H.; Asomoza, M. Structure of Borovanadate Glasses Studied by Raman Spectroscopy, *J. Non-Cryst. Solids.* **1997,** 210, 163-170.

[43] Kerkouri, N.; Haddad, M.; Et-tabirou, M.; Chahine, A.; Laanab, L. FTIR, Raman, EPR and Optical Absorption Spectral Studies onV_2O_5-Doped Cadmium Phosphate Glasses, *Physica B.* **2011,** 406, 3142-3148.

[44] Popovic, Z. V.; Konstantinovic, M. J.; Gajic, R.; Popov, V. N.; Isobe, M.; Ueda, Y.; Moshchalkov, V.V. Phonon Dynamics in AV_2O_5 .(*A*=Na,Ca,Mg,Cs) Oxides, *Phys. Rev. B.* **2002,** 65, 184303 1-8.

[45] Vedeanu, N.; Cozar, O.; Ardelean, I.; Lendl, B.; Magdas, D. A. Raman Spectroscopic Study of $CuO–V_2O_5–P_2O_5–CaO$ Glass System, *Vib. Spectrosc.* **2008,** 48, 259-262.

[46] Garbarczyk, J. E.; Machowski, P.; Wasiucionek, M.; Tykarski, L.; Bacewicz, R.; Aleksiejuk, A. Studies of Silver–Vanadate–Phosphate Glasses by Raman, EPR and Impedance Spectroscopy Methods, *Solid. State. Ionics.* **2000,** 136-137, 1077-1083.

[47] Lewandowska, R.; Krasowski, K.; Bacewicz, R.; Garbarczyk, J. E. Studies of Silver-Vanadate Superionic Glasses Using Raman Spectroscopy, *Solid. State. Ionics.* **1999,** 119, 229-234.

[48] Ramaraghavulu, R.; Sivaiah, K.; Buddhudu, S. Structural and Dielectric Properties of LiV_3O_8 Ceramic Powders, *Ferroelectrics.* **2012,** 432, 55-64.

[49] Chia, C. T.; Chen, Y. C.; Cheng, H. F.; Lin, I. Correlation of Microwave Dielectric Properties and Normal Vibration Modes of $xBa(Mg_{1/3}Ta_{2/3})O_3$–(1-x) $Ba(Mg_{1/3}Nb_{2/3})O_3$ Ceramics: I. Raman Spectroscopy, *J. Appl. Phys.* **2003,** 94, 3360-3364.

[50] Chen, M. Y.; Chia, C. T.; Lin, I.N.; Lin, L. J.; Ahn, C. W.; Nahm, S. Microwave Properties of $Ba(Mg_{1/3}Ta_{2/3})O_3$, $Ba(Mg_{1/3}Nb_{2/3})O_3$ and $Ba(Co_{1/3}Nb_{2/3})O_3$ Ceramics Revealed by Raman Scattering, *J. Eur. Ceram. Soc.* **2006,** 26, 1965-1968.

Figure captions

Fig. 1 TGA and DSC curves of stoichiometric mixture of a) $SrCO_3$-ZnO-V_2O_5 and b) $SrCO_3$-MgO-V_2O_5 ceramics

Fig. 2 Rietveld refinement and crystal structure of SZV ceramic

Fig. 3 Rietveld refinement and crystal structure of SMV ceramic

Fig.4 Raman spectra of a) SZV and b) SMV ceramics

Fig.5 Deconvoluted Raman spectra of SZV and SMV ceramics

Fig.6 Backscattered SEM images of a) SZV and b) SMV ceramics sintered at 660 and 780°C for 1h

Fig.7 Typical shrinkage behavior of SZV ceramics

Fig.8 CTE curves for SZV and SMV ceramics in the temperature range 30 to 300°C

Fig. 9 X-ray diffraction patterns of a) SZV+20% Al b) SZV+20% Ag sintered at 650°C for 1 h

Fig.10 a) Backscattered SEM image of SZV ceramic co-fired with 20wt% Al, b) EDS spectrum of spot 1, c) EDS spectrum of spot 2, (d) EDS line scan of SZV ceramic co-fired with 20wt% Al (e) X-ray dot mapping image of SZV ceramic co-fired with 20wt% Al

Fig. 11 a) Backscattered SEM image of SZV ceramic co-fired with 20wt% Ag, b) EDS spectrum of spot 1, c) EDS spectrum of spot 2, (d) EDS line scan of SZV ceramic co-fired with 20wt% Ag (e) X-ray dot mapping image of SZV ceramic co-fired with 20wt% Ag

Fig. 12 X-ray diffraction patterns of a) SMV ceramic and b) SMV ceramic co-fired with 20wt% Ag

Fig.13 a) Backscattered SEM image of SMV ceramic co-fired with 20wt% Ag, b) EDS spectrum of spot 1, c) EDS spectrum of spot 2, (d) EDS line scan of SMV ceramic co-fired with 20wt% Ag (e) X-ray dot mapping image of SMV ceramic co-fired with 20wt% Ag

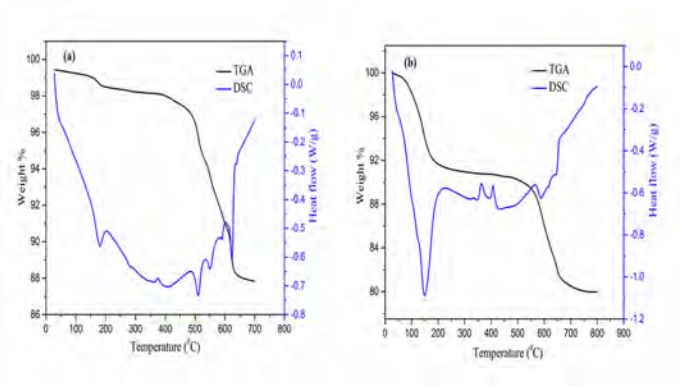

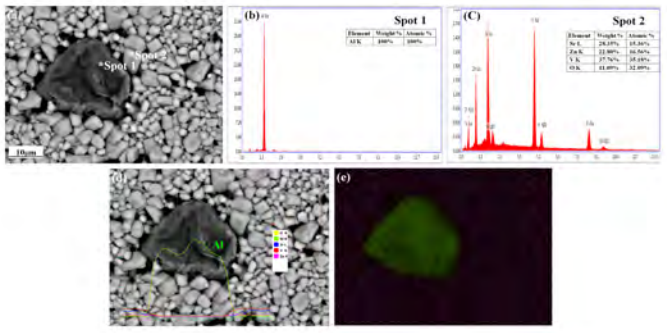

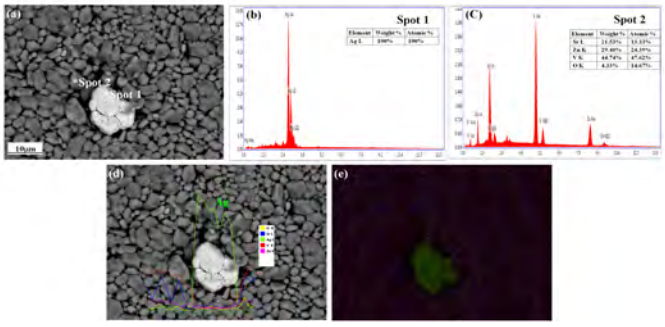

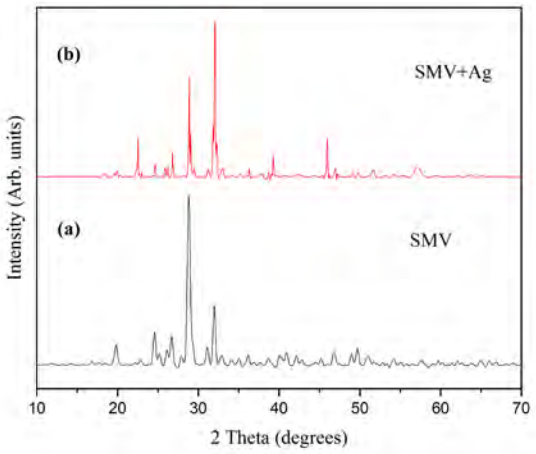

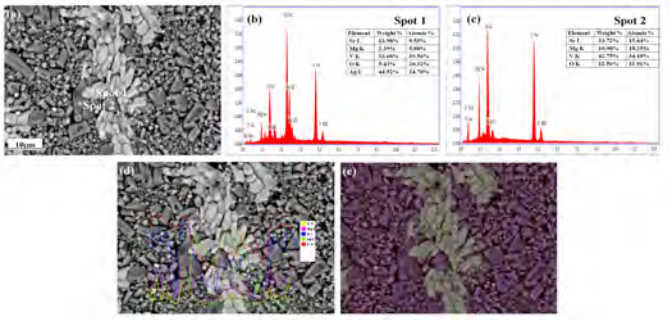

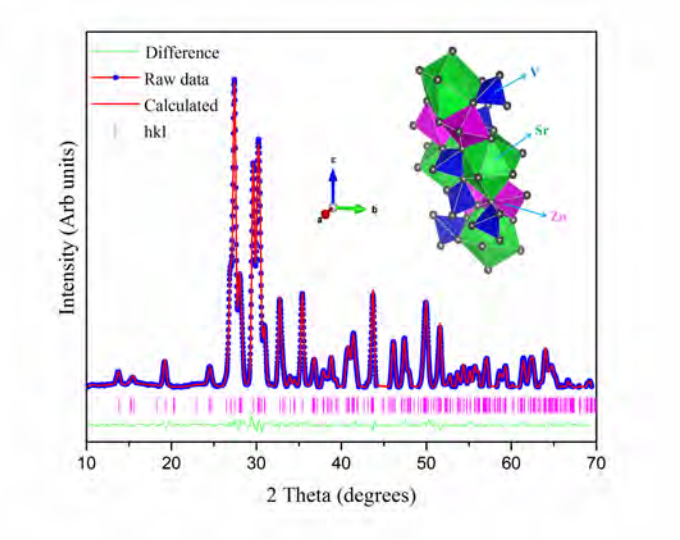

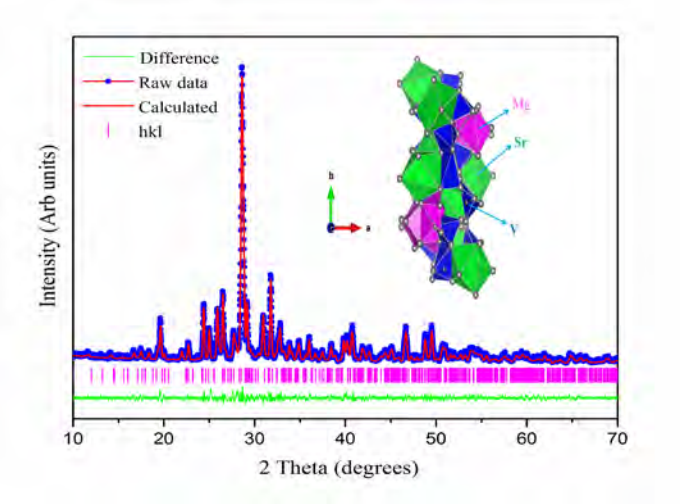

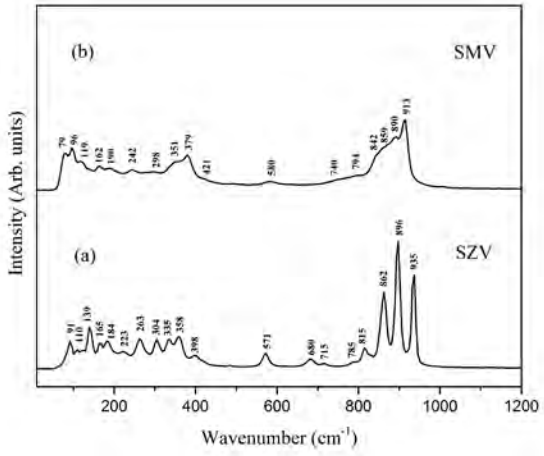

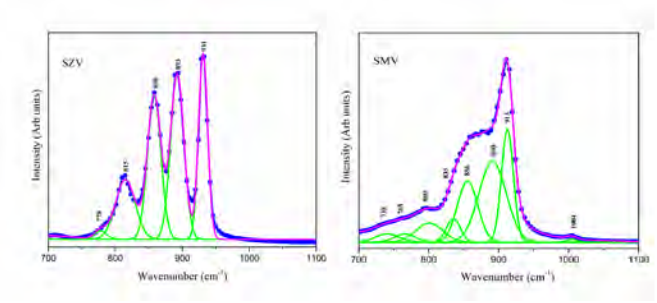

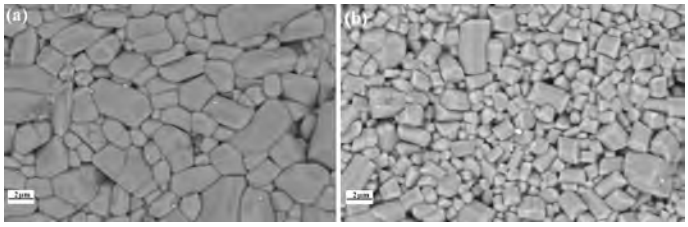

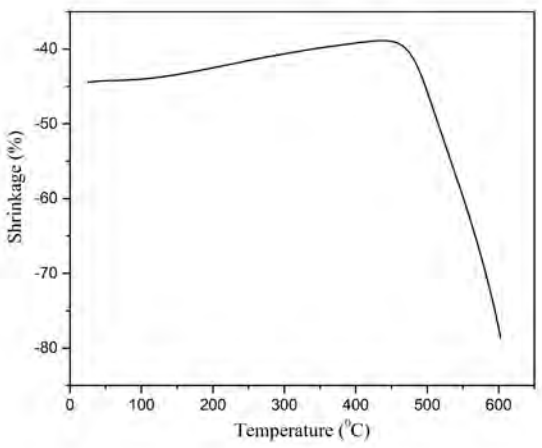

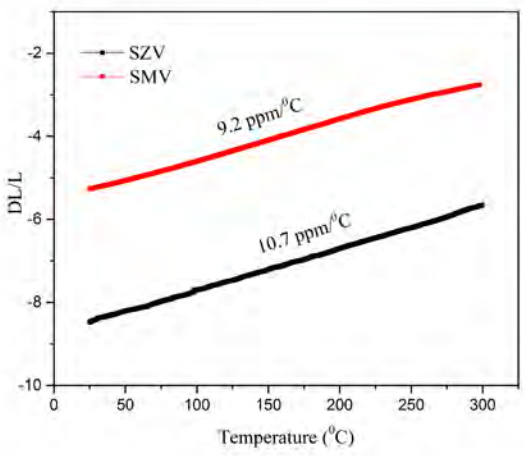

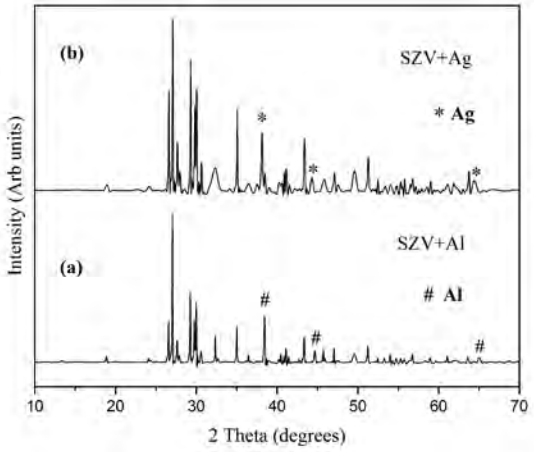

Highlights

- Preparation of glass free low temperature co-firable $SrMV_2O_7$ (M=Mg, Zn) ceramics
- Detailed structural studies using Rietveld refinement and Raman spectroscopy
- $SrMV_2O_7$ (M=Mg, Zn) ceramics show good microwave dielectric properties
- $SrZnV_2O_7$ ceramics exhibit excellent chemical compatibility with Ag and Al electrodes
- $SrZnV_2O_7$ ceramic can be used as potential candidate material for ULTCC applications